


Distinct sites on ABCA1 control distinct steps required for cellular release of phospholipids¹

Véronique Rigot,^{2,*} Yannick Hamon,* Olivier Chambenoit,* Mélanie Alibert,* Nicolas Duverger,[†] and Giovanna Chimini^{3,*}

Centre d'Immunologie de Marseille-Luminy,* INSERM/CNRS/Université de la Méditerranée, Parc Scientifique de Luminy, Case 906, 13288 Marseille Cedex 09, France; and Aventis Pharma,[†] 13 quai Jules Guesde, 94403 Vitry sur Seine, France

Abstract The loss of ABCA1 function leads to Tangier dyslipidemia in humans and to a Tangier-like phenotype in mice, by impairing the transformation of nascent apolipoproteins into mature HDL particles. Mechanistically this ensues from the inability of cells to release membrane lipids and cholesterol. Whereas the ability of ABCA1 to promote phospholipid effluxes, surface binding of apolipoproteins and outward flip of membrane lipids has been documented, the relationship between this series of ABCA1-dependent events is still elusive.  Here we provide evidence that *i*) lipid effluxes require both flip of membrane lipids and binding of apolipoproteins to the cell surface, *ii*) apolipoprotein A-I binding depends on structural determinants on ABCA1, and *iii*) phospholipid effluxes can be modulated by engineered mutations on the structural determinants identified on ABCA1.—Rigot, V., Y. Hamon, O. Chambenoit, M. Alibert, N. Duverger, and G. Chimini. Distinct sites on ABCA1 control distinct steps required for cellular release of phospholipids. *J. Lipid Res.* 2002. 43: 2077–2086.

Supplementary key words ABC transporter • lipid flipping • structure/function map • membrane topology • Tangier disease

The ATP Binding cassette transporter, ABCA1, controls the initial steps of reverse cholesterol transport, i.e., the release of cellular phospholipids (PL) to lipid-free apolipoproteins (1, 2). This has been unequivocally demonstrated by the study of Tangier patients (3–6), the naturally occurring loss-of-function model in humans, and by the targeted deletion of the ABCA1 locus in mice (7–9). In both cases, the level of circulating HDL cholesterol is highly reduced as a consequence of impaired cellular release of lipids from the membrane to their plasmatic acceptors (10, 11). This hampers the transformation of nascent lipid-free apolipoproteins into the centripetal cholesterol shuttle, the HDL particle. Molecular events required for the formation of a mature HDL particle in-

clude three successive steps (2). Surface docking of lipid-poor apolipoprotein, the core of the future HDL, is followed by the release from the cell surface of PL-enriched particles. These now assume the discoidal conformation permissive for cholesterol loading and maturation to spherical HDL. ABCA1 is considered to be rate limiting in the first two steps and indeed it has been demonstrated that the expression of ABCA1 promotes *i*) phosphatidylserine (PS) outward flipping at the plasma membrane, *ii*) apolipoprotein A-I (apoA-I) binding to the cell surface, and *iii*) cellular release of PL to nascent apolipoproteins (9, 12, 13); however, the temporal and causal relationship among the ABCA1-elicited cellular phenotypes is far from being ascertained. In order to gain insight into this complex phenomenon, we elaborated a structure-function map of the ABCA1 transporter. This analyzes the effect of naturally occurring missense mutations on the function of the transporter and is based on the assessment of ABCA1 membrane topology via a systematic epitope insertion approach. We present evidence here that a spectrum of molecular defects can generate a Tangier phenotype by interfering differently with the activity of the molecule. In particular, we could observe, on appropriately engineered molecules, a dissociation between the outward flipping of PS and the surface binding of apoA-I. Since the loss of either function leads to impaired PL effluxes, this demonstrates that both events are absolute prerequisites for PL loading of apoA-I and thus for HDL formation. In addition, by manipulating structural determinants on the ABCA1


Abbreviations: ER, endoplasmic reticulum; PL, phospholipids; PS, phosphatidylserine.

¹ Sequence sources are GI:13124694, GI:13123945, GI:18028983 for mouse, human, and chicken ABCA1; GI:6707663 and GI:6671495 for ABCR; GI:15451840 and GI:12656651 for ABCA7; GI:14916951 and GI:14916523 for ABCA2.

² V. Rigot and Y. Hamon contributed equally to the work.

³ To whom correspondence should be addressed.

e-mail chimini@ciml.univ-mrs.fr

 The online version of this article (available at <http://www.jlr.org>) contains an additional 2 tables.

Manuscript received 18 July 2002 and in revised form 16 September 2002.

Published, JLR Papers in Press, October 1, 2002.

DOI 10.1194/jlr.M200279JLR200

Copyright © 2002 by Lipid Research, Inc.

This article is available online at <http://www.jlr.org>

molecule specifically involved in the binding of apoA-I, we could revert hypomorphic mutant alleles to full function. This opens new therapeutic perspectives to modulate plasma HDL levels based on drug designed to improve the function of poorly performing ABCA1 alleles.

MATERIALS AND METHODS

Generation of informative constructs

All constructs were realized in pBI vector (Clontech). Double tagged constructs were generated by inserting, by overlap extension PCR (14), the HA epitope (YPYDVPDYA) on the already described ABCA1/EGFP backbone (9). In each case, an opportunistically chosen fragment was modified by amplification with two sets of primers spanning the restriction sites chosen for reinsertion of the fragment in the ABCA1/EGFP backbone (see supplementary material). In five cases, the HA tag was directly inserted into a natural or engineered restriction site on ABCA1 cDNA. Tangier missense mutations were similarly introduced by overlap extension PCR on an ABCA1/EGFP template (see supplementary material). The set of double tagged Tangier variants, possessing an HA tag at position 1433, was generated by introducing the *Sp/I-Sp/I* fragment from HA1433 into each Tangier backbone. $\Delta 60$ -ABCA1/EGFP construct was realized by mutating the third Tyr residue of the HA tag of the HA17 into a stop codon. Constructs, in all the insertion of HA and the specific substitutions on the wild type background were verified by sequencing with the Dynamic ET terminator Cycle sequencing kit (Amersham Pharmacia Biotech, Uppsala Sweden).

Transient transfection and assessment of intracellular traffic

HeLa cells were transiently transfected for 16 h with EXGEN 500 (Euromedex, Mundolsheim, France) accordingly to manufacturer's instruction and immediately seeded for immunofluorescence, biochemical, or functional analysis. Transfection efficiency is assessed by flow cytometric evaluation on a FACScalibur (Becton Dickinson) of the relative amount of transfected cells, i.e., expressing GFP and thus measured as EGFP RFI (relative fluorescence intensity) in the whole cell population. This was consistently higher than 30%. Intracellular trafficking was monitored by both immunofluorescence analysis and surface biotinylation at 60 h after transfection.

In the case of Tangier variants harboring both GFP and the HA tag at position 1433, dual channel flowcytometry was carried out at 60 h after transfection to monitor the amount of staining by the anti-HA antibody (clone 3F10, Roche, Mannheim, Germany) against the GFP signal.

Immunofluorescence was carried out by standard protocols on slides seeded with $3\text{--}5 \times 10^4$ cells and analyzed in X-Y dimensions by a Leica TS100 confocal microscope.

Immunoblot analysis was carried out on lysates from $3\text{--}5 \times 10^6$ cells treated with RIPA buffer (50mM Tris-HCl, pH:8, 150 mM NaCl, 1 mM EDTA and 1% Triton X-100) for 30 min at 4°C. Similar amounts of ABCA1, as normalized with respect to both protein concentration and transfection efficiency, were separated by SDS-PAGE and blotted for 20 h onto nitrocellulose sheets (Schleicher & Schuell, Dassel, Germany) according to standard protocols. The same membrane was subsequently hybridized with either the anti EGFP antibody (clone 7.1/13.1, Boehringer, Indianapolis) or the anti HA antibody (clone 3F10, Roche, Mannheim, Germany) followed by the appropriate anti-mouse or anti-rat HRP conjugated IgG (Jackson ImmunoResearch, Baltimore) and revealed by ECL (Amersham Pharmacia

Biotech, Uppsala Sweden). The stripping step was performed according to the protocol provided by the ECL manual.

Surface biotinylation was carried out on $3\text{--}5 \times 10^6$ cells with 1 mg/ml NHS-LC-biotin (Pierce) in ice cold PBS for 30 min, followed by lysis in RIPA buffer for 30 min at 4°C. Similar amounts of ABCA1, normalized as above, were immunoprecipitated with the anti EGFP antibody (clone 7.1/13.1), accordingly to standard protocols. The immunoprecipitated samples were fractionated by SDS PAGE and blotted for 20 h onto nitrocellulose paper (Schleicher & Schuell, Dassel, Germany). The biotinylated protein was then revealed by ECL after hybridization to streptavidine HRP (Amersham Pharmacia Biotech, Uppsala Sweden).

Functional analysis of transiently transfected cells

Fluorescence based assays for surface binding of cyanilated apoA-I or annexin V were carried out as described (12) at 60 h after transfection on $0.5\text{--}1 \times 10^6$ cells on a FACScalibur (Becton Dickinson) and analyzed by Flowjow software (Tree Star Inc., San Carlos, CA). Transfected cell, i.e., expressing GFP, and negative cells were manually gated and analyzed for Cy5 RFI as a measure of binding for ann-V or apoA-I. Results originated from transfected cells in each sample are expressed as a percent of the binding (mean of RFI) elicited by wild-type ABCA1/EGFP chimera transfected in parallel and then averaged from several individual experiments (n is shown in Table 2).

Lipid effluxes were assessed on 2×10^5 Cells seeded 24 h post transfection in 12 wells plates. After 24 h growth, cells were labeled for 8 h in a serum free medium containing 0.5% BSA, 1.5 $\mu\text{Ci/ml}$ ^{14}C -cholesterol (Amersham), and 10 $\mu\text{Ci/ml}$ ^3H -choline (Amersham). Cells were then washed twice in PBS-0.5%BSA, and effluxes were performed for 16 h to a 0.5% BSA serum free medium containing or not 10 $\mu\text{g/ml}$ apoA-I (Sigma). Cells were separated from medium and lipids were extracted (15). Radioactivity in the medium and cells was determined by liquid scintillation counting. The percentage of efflux is the count for the medium divided by the total count and each value is the average of four points. The efflux value was normalized according to the transfection efficiency evaluated by flowcytometry at the end of the experiment. Data, averaged from several experiments, are expressed as the percentage of the efflux generated by wild type ABCA1 transfected in parallel.

Statistical analysis to evaluate significance of the difference between samples and wild-type control was carried out by paired Student's *t*-test. When analyzing double mutants (HA819/C1477R and HA819/1466), the comparison was carried out between each double and the relevant loss of function single mutant (C1477R and HA1466, respectively).

RESULTS

Mapping extracellular regions on the ABCA1 transporter

A careful assessment of membrane topology is a prerequisite to establishing a structure function map of polytopic transporters such as ABCA1. To elucidate the position and length of regions exposed to the outer surface of the membrane, we constructed a panel of double tagged ABCA1 molecules. Each construct bears a fluorescent protein (FP; either YFP or EGFP) fused as a C-terminal tailpiece to the murine ABCA1 coding sequence. Such FP chimeras have already been validated as neutral to the folding on the basis of their unaltered subcellular target-

ing and function (9). A second tag in the form of an HA (hemalutinin) epitope was inserted at various positions along the ABCA1 coding sequence (Fig. 1). Two criteria dictated the selection of insertion sites. Computer-assisted prediction of transmembrane (TM) spanners was employed first to define loops connecting TM helices. The selected regions were further scanned for stretches of high variability by multi-alignment with the sequences of different members of the ABCA family (namely ABCA2, ABCR, ABCA7) (16). This restriction was expected to highlight regions under loose structural constraints; that is, likely to support the insertion of the heterologous HA nonamer without major consequences on the folding of the translated product.

The whole panel of constructions, schematized in Fig. 1A, was transiently expressed in HeLa cells and tested for expression by immunoblotting after surface biotinylation

(Fig. 1B). A morphological evaluation to assess intracellular localization and accessibility of the HA epitope was carried out in parallel by confocal laser microscopy (Table 1).

All the constructs were similarly and efficiently translated, but they differed markedly in their ability to reach the plasma membrane (Fig. 1B, Table 1, and Fig. 2, for an example of representative patterns). Out of the 14 constructs tested, seven showed an increased retention in the endoplasmic reticulum (ER) in comparison with the wild-type transporter. Only five of them (namely HA17, HA115, HA499, HA1345, and HA1615), however, failed to reach the membrane as assessed by both absence of surface biotinylation of the translated product and failure to visualize any plasma membrane localization by morphology (Figs. 1B and 2). This suggested a major impairment in the intracellular trafficking either due to misfolding uncensored by the ER quality control or to the inability to in-

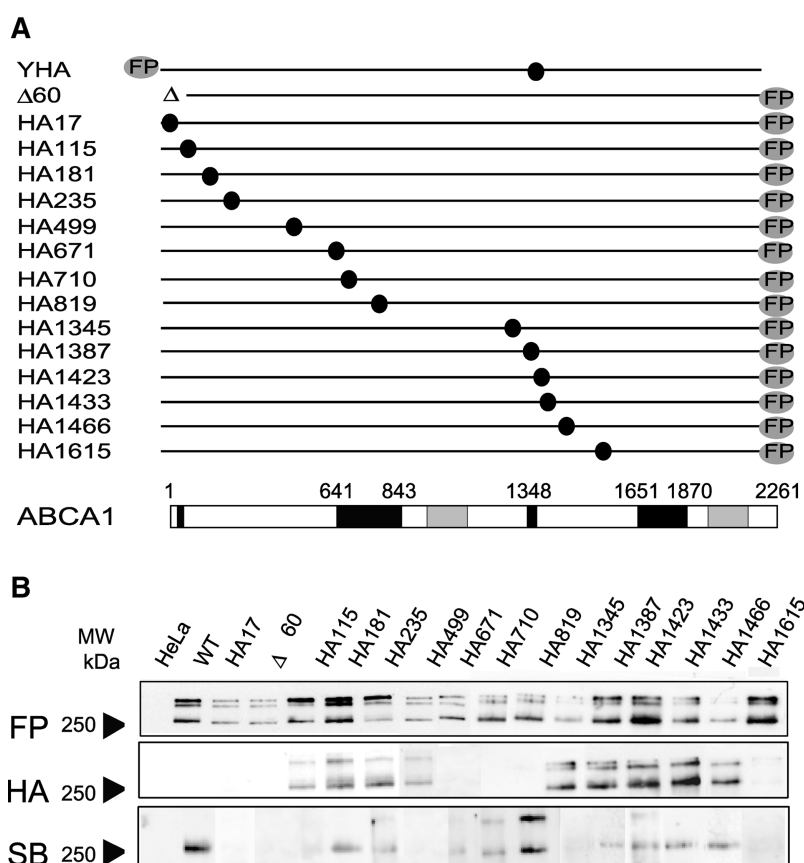


Fig. 1. A: Schematic representation of the panel of ABCA1 chimeras used in this study. The position of fluorescent proteins (YFP or EGFP) grafted either as C-terminal tailpiece or N-terminal extension is indicated (FP). The position of individual HA insertions is shown in each diagram (closed circles) and indicated in the name of the construct. A schematic representation of ABCA1 is also provided; the amino acid position with respect to the NBD (nucleotide binding folds in gray) and TM (transmembrane in black) is indicated. B: Analysis of expression and intracellular trafficking by immunoblotting with the GFP or HA specific antibody (indicated as GFP and HA respectively) and surface biotinylation (SB) of the chimeras transiently expressed in HeLa cells. Most of them are detected at the plasma membrane with large quantitative variations with respect to the control wild-type ABCA1/EGFP construct (WT). In six cases, virtually no protein is detectable on the cell surface while normally expressed, thus indicating a major folding/trafficking defect. The arrowhead shows the migration of the ABCA1/EGFP protein at ~250 kDa. The higher doublet detected in most samples corresponds to forms of higher molecular weight, possibly molecular aggregates of ABCA1. Their relative intensity varies as a function of the protein concentration in the samples.

TABLE 1. Compilation of morphological data from the whole panel of ABCA1 chimeras

Identity	Subcellular Localization	HA w/o P	HA w P
YHA1433	PM	+	+
$\Delta 60$	ER	—	—
HA17	ER	—	—
HA115	ER	—	+
HA181	PM	+	+
HA235	PM	+	+
HA499	ER	—	+
HA671	ER, PM	—	+
HA710	PM	—	—
HA819	PM	—	—
HA1345	ER, PM	—	+
HA1387	ER, PM	+	+
HA1423	PM	+	+
HA1433	PM	+	+
HA1466	PM	+	+
HA1615	ER	—	+/-

Subcellular localization as detected by confocal imaging and confirmed by surface biotinylation. Accessibility of HA epitope in the absence (w/o P) or presence (w P) of membrane permeabilization. ER, endoplasmic reticulum; PM, plasma membrane.

interact with a molecular chaperone. In the case of the other constructs, the translated product reached the plasma membrane. There the accessibility of the HA epitope was checked by staining with a specific antibody, either on fresh unfixed or on permeabilized transfected cells (Fig. 2). The tag inserted at position HA181, HA235, HA1387, HA1423, HA1433, and HA1466, was readily accessible to antibody staining on fresh unpermeabilized cells, thus indicating that these residues are located extracellularly. In contrast, the tag inserted at position 671 was accessible only after cell permeabilization, thus indicating that the loop between the hydrophobic helices TM2 (AA

640–662) and TM3 (681–703) is located intracellularly. Surprisingly, in three cases (HA17, HA710, and HA819) the HA epitope could not be detected by immunofluorescence in either condition nor by standard Western blotting in spite of normal detectability of the FP (Fig. 1B). Considering that in these cases the HA epitope is inserted in positions very close to the membrane itself (five residues from TM1 for HA17, seven from either TM3 or TM4 for HA710, and two from TM6 for HA819), it is possible that tight interactions with the lipid environment of the membrane bilayer hamper its detectability.

The N terminus

To address the controversial problem of the orientation of the N-terminus, we generated a $\Delta 60$ construct, driving the translation from Met+61 instead of Met+1, and two additional chimeras harboring the FP tag (YFP in this case) at the N terminus of either the wild-type ABCA1 or of an ABCA1 backbone tagged with HA at position 1433 (which we validated as neutral with respect to folding and function) (Fig. 1, Table 1 and Table 2). The deletion of the first 60 amino acids, which include the first predicted TM, leads to massive retention in the ER likely to be the cause of the reported lack of function of such truncated forms of ABCA1 (17). In contrast, the presence of a FP fusion at the N-terminus did not hamper the folding of the protein that reaches the plasma membrane (Fig. 3). We documented, in addition, that the N-terminal FP is not cleaved since both tags are detectable *i*) at the membrane, where they colocalize by confocal microscopy and *ii*) on a single protein product of the expected size by crossed immunoprecipitation and Western blotting on cell lysates (Fig. 3). Of note, the FP is accessible to staining by a

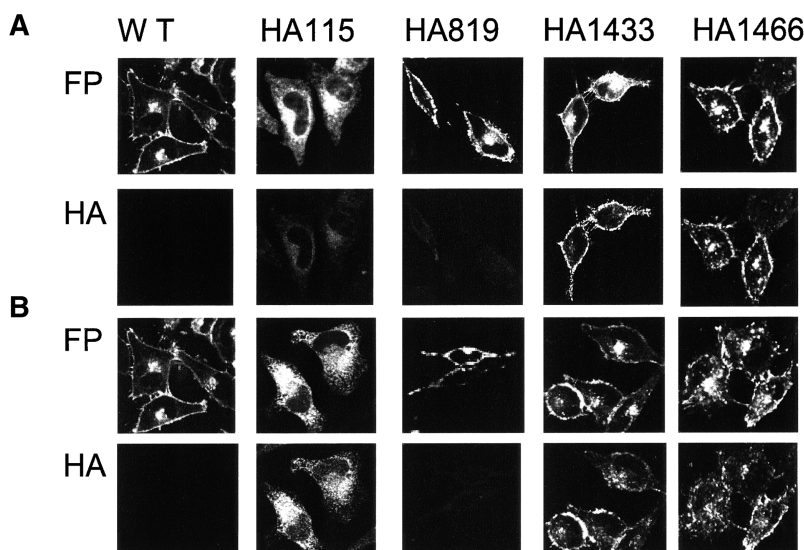


Fig. 2. Morphological and topological analysis of the HA/EGFP tagged ABCA1 chimeras. Confocal images of a representative set of chimeras are shown in both non permeabilized conditions (A series of panels) and in permeabilized conditions (B series of panels). The EGFP fluorescence pattern is shown in the upper lanes and compared with that of wild-type ABCA1/EGFP (WT). In the lower panels, the HA-specific immunostaining is shown. In the case of HA115, which is massively retained in the ER, this was detectable only after cell permeabilisation. The HA epitope was accessible to staining on fresh cells both in the case of HA1433 and HA1466. The HA tag inserted at position HA819 was undetectable in either condition.

TABLE 2. Functional evaluation of the panel of HA/ABCA1 chimeras

Identity	AnnV	St	ApoA-I	St	PL Efflux	St
	%		%		%	
YHA1433	98 ± 21 (2)	ns	101 ± 1 (2)	ns		
Δ60	21 ± 11 (4)	^a	9 ± 2 (2)	^c		
HA17	17 ± 17 (2)	^a	3 ± 4 (3)	^c		
HA115	13 ± 7 (5)	^c	29 ± 5 (3)	^c		
HA181	110 ± 14 (7)	ns	102 ± 15 (6)	ns		
HA235	105 ± 17 (3)	ns	84 ± 7 (3)	ns		
HA499	26 ± 6 (3)	^b	16 ± 10 (2)	^b		
HA671	51 ± 20 (4)	ns	9 ± 8 (5)	^c		
HA710	49 ± 3 (2)	^a	17 ± 15 (3)	^a		
HA819	109 ± 31 (7)	ns	151 ± 11 (4)	^a	113 ± 24 (4)	ns
HA1345	11 ± 3 (4)	^c	16 ± 6 (2)	^b		
HA1387	34 ± 17 (3)	ns	46 ± 13 (3)	^a		
HA1423	98 ± 6 (2)	ns	91 ± 10 (5)	ns		
HA1433	96 ± 18 (5)	ns	88 ± 25 (6)	ns		
HA1466	52 ± 10 (7)	ns	27 ± 7 (9)	^c	35 ± 15 (3)	^a
HA1615	12 ± 7 (4)	^b	1 ± 1 (2)	^c		

AnnV and ApoA-I, binding of annexin V or apoA-I in cells successfully transfected with the test construct (GFP positive); St, statistical significance. Binding is expressed as percent of the binding elicited by the wild-type construct (considered as 100%). Details on the calculation are reported in Materials and Methods. Values represent the mean ± SEM. In brackets is shown the number of individual experiences. *P* values calculated by two-tailed Student's *t*-test. The comparison was carried out between the mutant and the control wild-type values.

^a *P* < 0.05.

^b *P* < 0.01.

^c *P* < 0.001.

specific antibody only after cell permeabilisation (not shown). These findings, therefore, provide further evidence that the N terminus of ABCA1 is intracellular and that the first transmembrane helix at position 23–44 behaves as a signal anchor (18, 19).

An overall analysis of the topological data outlined above is consistent with the model proposed in Fig. 4A. This confirms the already suggested presence of a large extracellular loop (from residue 44 to 640) (18, 19) an-

chored to the plasma membrane by the first uncleaved TM (23–44) (19), and proposes the existence of a second extracellular loop (from 1,368 to 1,651) symmetrically positioned in the second half of the transporter between TM7 and TM8.

Functional analysis of the informative constructs

To further validate our approach, we checked the functionality of these chimeras via fluorescence based assays assessing two ABCA1-associated activities: the ability to induce the flip of PS in the outer membrane leaflet of expressing cells, measured by binding of Cy5 annexin V, and the ability to elicit surface binding of Cy5 apoA-I (9, 12) (Table 2).

All the chimeras retained in the ER failed to elicit any significant surface binding of both apoA-I and annexin V (as an example of this situation, the results obtained with HA115 are shown in Fig. 5). This is consistent with the idea that the presence of the transporter at the plasma membrane is required to elicit both these events.

The chimeras correctly targeted to the plasma membrane differed markedly in their functional behavior in either or both assays (an example is given in Fig. 5 and all the results are summarized in Table 2). The insertion of an HA tag at positions 819 (Fig. 5), i.e., between TM 5 and 6, is not only devoid of negative effects on function but rather induces a significant increase with respect to wild-type ABCA1 of apoA-I surface binding (151% ± 11; *n* = 4, *P* < 0.05) but not of annexin V (109% ± 31; *n* = 7, *P* > 0.05). The HA tag inserted at position 181, 235, 1423, 1433 did not hamper function as assessed by both apoA-I binding and PS flipping (as an example, HA1433 is shown in Fig. 5). The chimeras bearing an HA insertion at position 671, 710, 1387, and 1466 (shown as an example in Fig. 5), albeit targeted to the plasma membrane, showed a significant reduction in the ability to elicit apoA-I binding associated with variable degrees of impairment

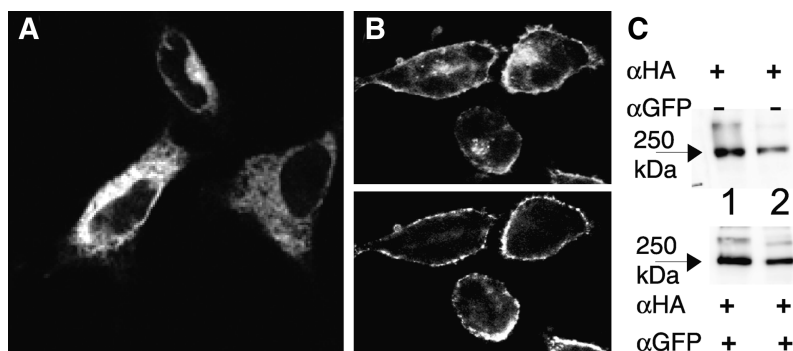


Fig. 3. Analysis of the N-terminal domain of ABCA1. A: Confocal images of EGFP fluorescence in cells transfected with Δ60 construct show that the protein translated from Met+61 is retained in the ER. This indicates that the first hydrophobic segment 23–44 is required for folding and/or trafficking. B: Confocal images of cells transfected with the YFP/HA1433 ABCA1 chimera show that both YFP (upper) and the HA (lower) staining colocalize at the plasma membrane. Of note, the FP is detected by a specific antibody only after cell permeabilisation (not shown), whereas HA is detectable on fresh cells. C: Lysates from cells transiently transfected with HA1433 bearing EGFP at the C terminus (lane 1) or YFP HA1433, i.e., grafted with YFP at the N-terminus (lane 2), were either directly blotted onto membrane and probed with an anti-HA antibody (upper panel) or immunoprecipitated with an anti-GFP antibody before blotting and probed with the HA antibody. In both cases, the expressed protein product is detected by the two antibodies, thus indicating that the N-terminal FP is uncleaved.

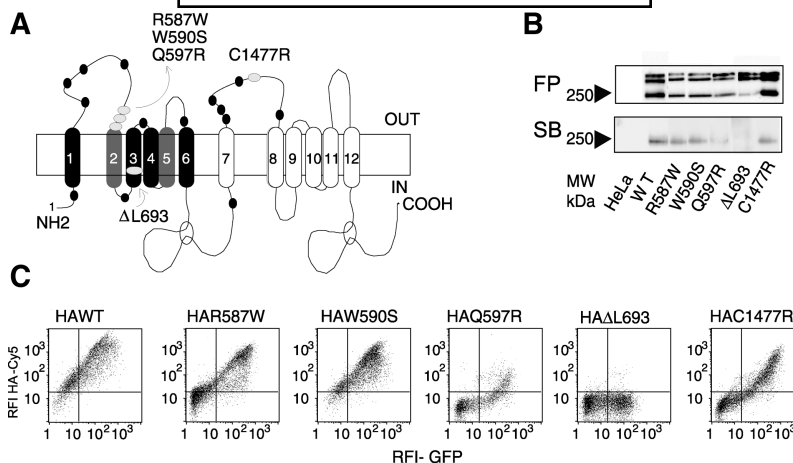


Fig. 4. The proposed model for ABCA1 topology is shown in A. Two symmetrical halves are present. The respective putative TM spanners are numbered and identified in gray for the N-terminal half and in white for the C-terminal one. The limits of each predicted TM are: 25 to 42 for TM1, 639 to 656 for TM2, 679 to 704 for TM3, 681 to 704 for TM4, 749 to 765 for TM5, 818 to 842 for TM6, 1,346 to 1,369 for TM7, 1,655 to 1,677 for TM8, 1,696 to 1,722 for TM9, 1,735 to 1,759 for TM10, 1,766 to 1,788 for TM11, and 1,853 to 1,870 for TM12. The position of HA insertions is shown as black dots. Empty dots indicate the position of amino acid substitutions described in pedigrees of Tangier patients and selected for this study. B: Shows the analysis of expression by immunoblotting with a GFP specific antibody (FP) and of membrane localization by surface biotinylation (SB) of the ABCA1 Tangier variants expressed in HeLa. Q597R and ΔL693 are virtually absent from the cell surface while expressed normally. For comparison wild-type ABCA1/EGFP is shown (WT). The arrowhead shows the migration of the ABCA1/EGFP protein. C: Shows dual channel flowcytometric recording of the whole set of Tangier variants equipped with an HA tag at position 1433, i.e., extracellular and devoid of interference with intracellular trafficking and function of the transporter. For comparison, the behavior of the HA1433 (HAWT) is shown.

in PS flipping (Table 2). These results, although not conclusive by themselves, hinted that PS flipping could be dissociated from apoA-I binding by the targeting of selected domains on the transporter.

Tangier missense mutations impair ABCA1 function at discrete checkpoints

To progress in our interpretation, we chose then to investigate the functional behavior of selected point mutations. Several mutations have been reported in Tangier disease patients, the naturally occurring human model for ABCA1 loss of function (3–6, 20). Most of them, however, are null alleles due to premature truncations of the coding sequence, thus inadequate for structure/function analysis. To fine tune our study, we needed ABCA1-mutant alleles bearing a single amino acid substitution or deletion. Those should be translated into complete proteins whose functional behavior can be assessed. We deliberately excluded mutations in the nucleotide binding folds, i.e., those expected to impair function by interference with the ATPase activity, and conversely selected the mutations located in the extracellular region defined by the topological model proposed in Fig. 4A.

Three point mutations in the region 580–600 had been reported in Tangier pedigrees (namely R587W, W590S, and Q597R). These are located in the large loop in between TM1 and TM2. They were introduced by PCR-directed mutagenesis on an ABCA1/EGFP backbone. Two additional mutants were similarly generated. They harbor

a substitution at position 1477, i.e., in the second large extracellular loop between TM7 and TM8 and the deletion of leucine 693 in TM3 (4). It is of note that all the substitutions concern residues conserved in human, mouse, and chicken ABCA1.

The five engineered constructs were transfected and tested by biochemical, morphological, and functional criteria (Fig. 4, Fig. 6, and Table 3). In all cases, a significantly reduced PL efflux from expressing cells was evidenced. This was virtually complete in the case of W590S, Q597R, and ΔL693, and reduced to one fourth for R587W and C1477R (Table 3).

Since, however, dramatic differences in intracellular trafficking were detected by both biochemical and morphological analysis, a second set of constructs was generated. These, harboring an HA tag at position 1433, i.e., exposed extracellularly and devoid of interference with the function of the transporter, allow us to document upon transfection the appearance at the cell surface of GFP chimeras by monitoring the signal obtained with an anti-HA antibody as a function of GFP fluorescence. This dual channel flowcytometry analysis, shown in Fig. 4C for the whole set of variants, further corroborated the previously detected differences in intracellular routing.

The pathognomonic sign of Tangier disease, i.e., inadequate PL effluxes, originates in fact from fairly different behaviors exemplified by three categories.

Two of the Tangier transporters (namely Q597R and ΔL693) reach the plasma membrane very inefficiently, and as a consequence fail to elicit any significant function as measured by surface binding of either annexin V or

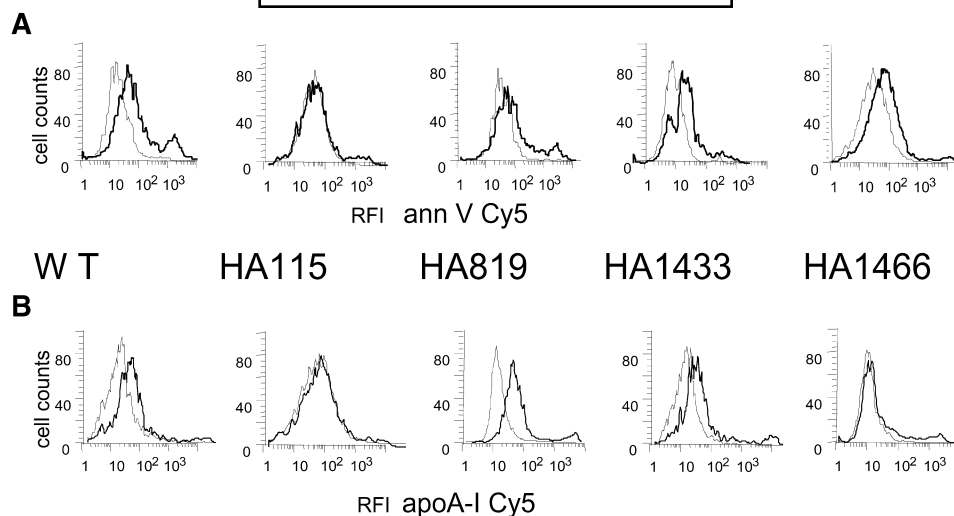


Fig. 5. Functional assessment of the informative ABCA1HA/EGFP constructs transiently expressed in HeLa cells. The binding of Cy5 labeled annexin V (upper panel) and of Cy5 apolipoprotein A-I (apoA-I) (lower panel) on the cell surface is shown as a function of EGFP expression. Thick lines, representing EGFP expressing cells, are compared with non transfected, EGFP negative cells (thin line). In each panel, the behavior of cells expressing wild-type ABCA1/EGFP (WT) is shown for comparison. A representative flowcytometry profile (out of several individual experiments) is shown for each construct. The values (average shift of the mean RFI as percent of wild type shift \pm SE) obtained for all the constructs and the statistical significance of variations are summarized in Table 2.

apoA-I. Here a major trafficking defect is at the basis of the Tangier phenotype.

C1477R falls into a second class since it is detected at the plasma membrane but elicits a significantly reduced binding of apoA-I as compared with wild-type ($33\% \pm 9$, $n = 6$, $P < 0.01$ Table 1). This is accompanied by a modest and non significant decrease in annexin V binding ($53\% \pm 12$, $n = 9$, $P > 0.05$) and by significantly lower PL effluxes ($12\% \pm 2$, $n = 2$, $P < 0.01$), thus suggesting that the main defect resides in the inability to elicit apoA-I docking in line with the currently accepted paradigm.

The last category is illustrated by R587W and W590S Tangier transporters, which are correctly targeted to the plasma membrane, but show a marked functional dissociation. Indeed, these variants, while eliciting an apoA-I binding indistinguishable from wild-type ABCA1 ($79\% \pm 5$, $n = 7$, $P > 0.05$ and $126\% \pm 18$, $n = 6$, $P > 0.05$ of wild type, respectively) fail to drive both flipping of PS (annexin V binding = $39\% \pm 11$ of wild type for R587W, $n = 5$, $P < 0.05$ and $30\% \pm 9$ for W590S, $n = 7$, $P < 0.01$) and membrane release of PL ($27\% \pm 16$, $n = 3$, $P < 0.05$ and $16\% \pm 3$, $n = 2$, $P < 0.01$ of wild type, respectively, Table 3), thus indicating that apoA-I binding per se is insufficient for the generation of PL effluxes, which also requires PS flipping.

HA 819 acts as a suppressive mutations on Tangier C1477R

Having observed that we could generate mutant transporters showing opposite behaviors with respect of apoA-I surface binding, we asked which effect could result from the introduction of a gain of function mutation on an hypomorphic mutant allele. We thus grafted the HA819, which increases selectively apoA-I binding ($151\% \pm 11$ of wild type, $n = 4$, $P <$

0.05), on HA1466 (apoA-I binding = $27\% \pm 7$ of wild type, $n = 9$, $P < 0.001$), and on C1477R ($33\% \pm 9$ of wild type, $n = 6$, $P < 0.01$). The latter showed similar levels of annexin V binding ($52\% \pm 10$, $n = 7$ for HA1466 $P > 0.05$ and $53\% \pm 12$, $n = 9$, for C1477R, $P > 0.05$).

Although differently engineered, these latter constructs concern proximate residues at position 1466 and 1477 and result in quite similar functional defects in that both lead to an impaired PL efflux accompanied by a reduced ability to bind apoA-I (Tables 2 and 3). The double mutants were then tested functionally. In both cases, the presence of an HA tag at position 819 partially and significantly rescued the binding of apoA-I but drove limited and nonsignificant modifications in the annexin V binding with respect to the original loss of function mutation (Table 3; apoA-I binding values reverted to $68\% \pm 6$ for HA819/C1477R, $n = 4$, $P < 0.05$ and to $49\% \pm 7$ for HA819/HA1466, $n = 6$, $P < 0.05$, whereas annexin V binding amounted to $57\% \pm 15$, $n = 4$, for HA819/C1477R and $54\% \pm 12$, $n = 6$ for HA819/HA1466 $P > 0.05$). In both cases the ability to induce PL effluxes was also significantly increased (HA819/C1477R = $142\% \pm 24$, $n = 2$, $P < 0.01$ and HA819/HA1466 = $108\% \pm 28$, $n = 4$, $P < 0.05$). This indicates that in the presence of an adequate PS flipping, the increase in apoA-I binding directly influences cellular lipid effluxes.

DISCUSSION

The data presented here provide a novel insight into some aspects of the molecular function of the ABCA1 transporter with major physiopathological implications.

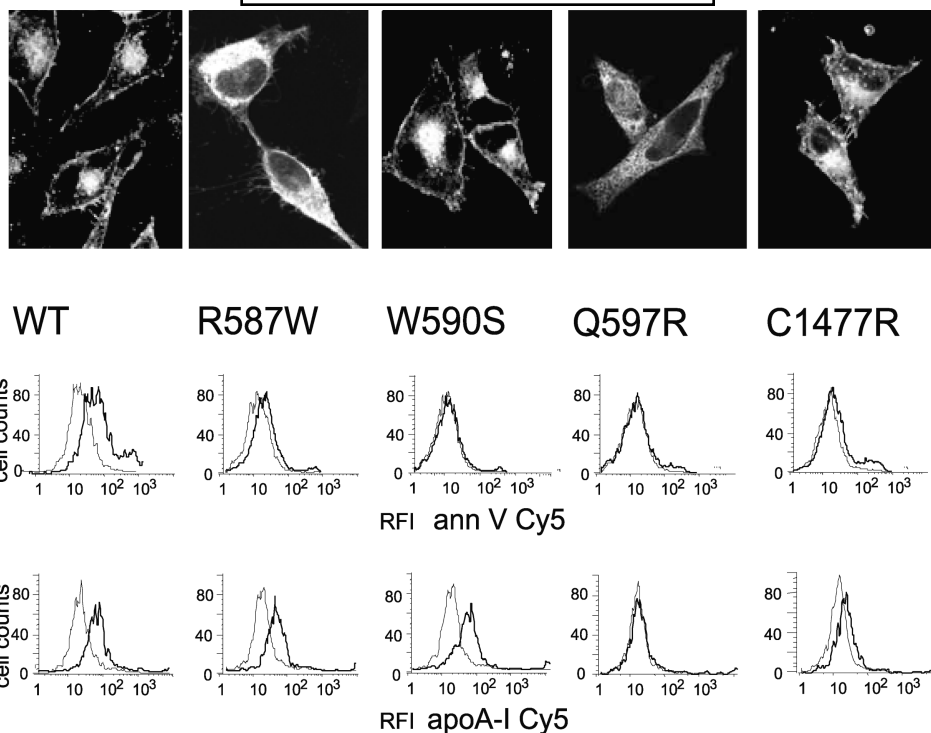


Fig. 6. Morphological and functional analysis of ABCA1 variants associated with Tangier phenotype. Confocal images of ABCA1 mutant alleles expressed in HeLa cells (upper panel) indicate that in the case of Q597R the mutation affects intracellular trafficking and leads to retention into the ER. A similar defect is found in the case of Δ L693 (not shown). In the other cases, the substitution does not hamper the targeting to the plasma membrane. The lower panel shows a representative FACS profile assessing the functionality of each mutant by annexin V binding or apoA-I binding as detailed in the legend to Fig. 5. Table 3 summarizes the functional data obtained.

The first issue concerns the membrane topology of ABCA1. By the use of an epitope insertion approach, we provide a model of ABCA1 arrangement at the plasma membrane schematized in Fig. 4A. This predicts a symmetrical protein with a short intracellular N terminus followed by a first TM helix anchoring a large extracellular loop; a similar architecture is proposed for the second half of the protein starting from the putative TM spanner, previously called HH1 (21), which acts as an in-to-out seventh TM helix. This model is perfectly consistent with the topological arrangement recently assessed by the mapping of glycosylation sites (19, 22) and corroborates then the hypothesis that all the ABC transporters belonging to the A class share a similar topology (23).

The intracellular positioning of the N terminus and its presence in the final product is consistent with the results of Fitzgerald (19) and the prediction based on homology to ABCR (23, 24). It is nonetheless in conflict with the results of Tanaka (18), indicating that the first TM is cleaved and acts as a signal peptide. The latter conclusion was principally supported by the inability to detect the HA epitope fused at the N terminus of ABCA1 by Western blotting. In our case, the use of FP as a tag and the combination of both biochemical and morphological evidence has allowed to clarify the issue.

We could, in addition, by the coupled topological and functional analysis of naturally occurring ABCA1 mutant

alleles, document that multiple molecular defects ensue in a Tangier phenotype are defined as the inability to induce membrane release of PL.

The first checkpoint is at the level of intracellular routing

TABLE 3. Morphological and functional evaluation of Tangier-associated ABCA1 variants

Identity	SL	AnnV	St	ApoA-I	St	PL Efflux	St
		%		%		%	
R587W	PM	39 \pm 11 (5) ^a		79 \pm 5 (7) ^a		27 \pm 16 (3) ^a	
W590S	PM	30 \pm 9 (7) ^b		126 \pm 18 (6) ns		16 \pm 3 (2) ^b	
Q597R	ER, PM	24 \pm 9 (4) ^b		15 \pm 8 (4) ^c		8 \pm 7 (2) ^b	
Δ L693	ER	26 \pm 11 (5) ^a		12 \pm 6 (4) ^c		nd	
C1477R	PM	53 \pm 12 (9) ns		33 \pm 9 (6) ^b		12 \pm 2 (2) ^b	
HA819/1466	PM	54 \pm 12 (6) ns		49 \pm 7 (6) ^a		108 \pm 28 (4) ^b	
HA819/C1477R	PM	57 \pm 15 (4) ns		68 \pm 6 (4) ^a		142 \pm 24 (2) ^b	

SL, subcellular localization as detected by confocal imaging and confirmed by surface biotinylation; AnnV and ApoA-I, binding of annexin V or apoA-I in cells successfully transfected with the test construct (GFP positive); St, statistical significance. Binding is expressed as percent of the binding elicited by the wild-type construct (considered as 100%). Details on the calculation are reported in Materials and Methods. Values represent the mean \pm SEM. In brackets is shown the number of individual experiences. *P* values calculated by two tailed Student's *t*-test. In the case of the double mutants the comparison was carried out between the double and the single mutant leading to loss of function, in all other cases comparisons were carried out against the control wild-type values.

^a *P* < 0.05.

^b *P* < 0.01.

^c *P* < 0.001.

ing; indeed, the failure to reach the plasma membrane leads consistently to loss of function. This finding, which reproduces the case of the $\Delta F508$ in the CFTR transporter, i.e., the most common mutation causing cystic fibrosis (25), indicates that efficient cellular release of PL requires the presence of a functional ABCA1 at the plasma membrane.

A different situation is illustrated by the ABCA1 variants, which, albeit correctly targeted, show decreased functionality. There the loss of PL effluxes can result from either defective PS flipping or reduced apoA-I binding. Whereas a direct causal relationship between apoA-I binding levels and effluxes is not surprising, this is the first report pointing out that the isolated absence of PS flipping is associated with inefficient cellular release of PL. This data clearly indicate that apoA-I binding is not in itself sufficient to drive lipid loading of apolipoproteins but that this latter also requires the membrane destabilization characterized by the outward PS flip. These results are in apparent contrast with those of Smith, who, while confirming that the presence of ABCA1 leads to exposure of PS, could not find a direct functional correlation between the outward flip of PS and cholesterol effluxes (26); however, it has to be pointed out that they tested the correlation during PS exposure induced by apoptosis. This cannot be considered equivalent to the physiological ABCA1-dependent model, which is consistently dissociated from the major cellular dismantling accompanying cell death (9, 12). In addition, our results provide an adequate explanation for the lack of lipid effluxes in cells still able to efficiently bind apoA-I. This is the case of the Tangier variant W590S, whose behavior has also been documented by Fitzgerald et al. (22).

Several implications stem from these results. They bring indirect support to the hypothesis that ABCA1 plays a key role in the formation of circulating HDL particles when nascent apolipoproteins are available in large amounts (27). This would be consistent with the *in vivo* results, suggesting that the maintenance of HDL plasma levels depends only minimally on ABCA1 in macrophages, cells theoretically in contact with negligible amounts of nascent apolipoproteins (28).

Further extrapolating along the same line of thought, PS flipping could be coupled to alternative dockings of yet unknown molecules in macrophages, but also in other dedicated cell lineages (29). This may be at play for instances of the phagocytosis of apoptotic corpses, a second homeostatic circuit under the influence of ABCA1 (9, 30).

Finally, these results provide, in essence, the molecular clues to the variable penetrance of clinical signs in Tangier pedigrees (10). Given molecular defects borne by specific ABCA1 mutant alleles may, in fact, account for clinical variability.

A last set of conclusions is linked to the observed dissociation between the two ABCA1-dependent functions explored in this study. This, by defining structural determinants strategic for the surface binding of apolipoproteins, may support the previous suggestions of their physical contact with ABCA1 (13, 31); however, it cannot be ex-

cluded that the interaction between ABCA1 and apoA-I is indirect and dependent on both an intact ATPase activity of the transporter and the presence of structural determinants (12, 13).

In particular, the results obtained with both tagged and single mutant molecules indicate that residues proximate to position 1477, in the second large extracellular loop, are crucial for apoA-I docking at the cell surface but devoid of major incidence on flippase activity. Of note residue 1477 is a cysteine. Since the presence of disulfide bridges connecting the two halves of the protein has been shown for ABCR and, by extension, suggested for ABCA1, C1477 may well be strategic for the structural configuration of extracellular domains (23); however, considering that the loss of apoA-I binding in C1477R can be rescued by a suppressive mutation in the loop between TM5 and TM6 unable in itself to restore a disulfide bridge, it seems more likely that the coexistence of two discrete modifications in the putative apoA-I docking domain can fine tune its spatial conformation. Moreover, the fact that the presence on the same ABCA1 molecule of two mutations with opposite effects leads to suppression of the defect borne by the hypomorphic one and to complete functional recovery conveys potential clinical implications. Indeed, it reveals that novel strategies of drug-design targeted to conformational modifications of the apolipoprotein/ABCA1 contact groove can be developed. These will be particularly appropriate to increasing the functionality of ABCA1 alleles which, while not leading to overt Tangier phenotype, are associated to a reduction of plasma HDL levels (32–34) and thus to an increased risk for cardiovascular disease (35, 36). ■

The authors wish to thank J. M. Freyssinet for having provided recombinant annexin V and P. Golstein for discussion. This work was financially supported by institutional grants from CNRS and INSERM; and by specific grants from AVENTIS-Pharma, Vaincrelamucoviscidose, and Fondation de France. V.R. was supported by a fellowship from Vaincrelamucoviscidose.

REFERENCES

1. Tall, A. R., and N. Wang. 2000. Tangier disease as a test of the reverse cholesterol transport hypothesis. *J. Clin. Invest.* **106**: 1205–1207.
2. Fielding, P. E., K. Nagao, H. Hakamata, G. Chimini, and C. J. Fielding. 2000. A two-step mechanism for free cholesterol and phospholipid efflux from human vascular cells to apolipoprotein A-I. *Biochemistry*. **39**: 14113–14120.
3. Bodzioch, M., E. Orso, J. Klucken, T. Langmann, A. Böttcher, W. Diederich, W. Drobnik, S. Barlage, C. Büchler, M. Porsch-Özcürümez, W. E. Kaminski, H. W. Hahmann, K. Oette, G. Rothe, C. Aslanidis, K. J. Lackner, and G. Schmitz. 1999. The gene encoding ATP-binding cassette transporter 1 is mutated in Tangier disease. *Nature Genet.* **22**: 347–351.
4. Brooks-Wilson, A., M. Marcil, S. M. Clee, L. H. Zhang, K. Roomp, M. van Dam, L. Yu, C. Brewer, J. A. Collins, H. O. Molhuizen, O. Loubser, B. F. Ouellette, K. Fichter, K. J. Ashbourne-Excoffon, C. W. Sensen, S. Scherer, M. Mott, M. Denis, D. Martindale, J. Frohlich, K. Morgan, B. Koop, S. Pimstone, J. J. Kastelein, J. Genest, Jr., and M. R. Hayden. 1999. Mutations in ABC1 in Tangier dis-

ease and familial high-density lipoprotein deficiency. *Nature Genet.* **22**: 336–345.

5. Lawn, R. M., D. P. Wade, M. R. Garvin, X. Wang, K. Schwartz, J. G. Porter, J. J. Seilhamer, A. M. Vaughan, and J. F. Oram. 1999. The tangier disease gene product ABC1 controls the cellular apolipoprotein-mediated lipid removal pathway. *J. Clin. Invest.* **104**: R25–31.
6. Rust, S., M. Rosier, H. Funke, J. Real, Z. Amoura, J. C. Piette, J. F. Deleuze, H. B. Brewer, N. Duverger, P. Deneffe, and G. Assmann. 1999. Tangier disease is caused by mutations in the gene encoding ATP-binding cassette transporter 1. *Nature Genet.* **22**: 352–355.
7. Christiansen-Weber, T. A., J. R. Volland, Y. Wu, K. Ngo, B. L. Roland, S. Nguyen, P. A. Peterson, and W. P. Fung-Leung. 2000. Functional loss of ABCA1 in mice causes severe placental malformation, aberrant lipid distribution, and kidney glomerulonephritis as well as high-density lipoprotein cholesterol deficiency. *Am. J. Pathol.* **157**: 1017–1029.
8. McNeish, J., R. J. Aiello, D. Guyot, T. Turi, C. Gabel, C. Aldinger, K. L. Hoppe, M. L. Roach, L. J. Royer, J. de Wet, C. Broccardo, G. Chimini, and O. L. Francone. 2000. High density lipoprotein deficiency and foam cell accumulation in mice with targeted disruption of ATP-binding cassette transporter-1. *Proc. Natl. Acad. Sci. USA.* **97**: 4245–4250.
9. Hamon, Y., C. Broccardo, O. Chambenoit, M. F. Luciani, F. Toti, S. Chaslin, J. M. Freyssinet, P. Devaux, J. Neish, D. Marguet, and G. Chimini. 2000. ABC1 promotes engulfment of apoptotic cells and transbilayer redistribution of phosphatidylserine. *Nat. Cell Biol.* **2**: 399–406.
10. Assmann, G., A. von Eckardstein, and H. B. Brewer. 2001. Familial analphalipoproteinemia: tangier disease. In *The Metabolic Basis of Inherited Disease*. C. R. Scriver, A. L. Beaudet, W. S. Sly, D. Valle, editor. McGraw-Hill, New York. 2937–2960.
11. Remaley, A. T., U. K. Schumacher, J. A. Stonik, B. D. Farsi, H. Nazih, and H. B. Brewer, Jr. 1997. Decreased reverse cholesterol transport from Tangier disease fibroblasts. Acceptor specificity and effect of brefeldin on lipid efflux. *Arterioscler. Thromb. Vasc. Biol.* **17**: 1813–1821.
12. Chambenoit, O., Y. Hamon, D. Marguet, H. Rigneault, M. Rosse-neu, and G. Chimini. 2001. Specific docking of apolipoprotein A-I at the cell surface requires a functional ABCA1 transporter. *J. Biol. Chem.* **276**: 9955–9960.
13. Wang, N., D. L. Silver, C. Thiele, and A. R. Tall. 2001. ABCA1 functions as a cholesterol efflux regulatory protein. *J. Biol. Chem.* **276**: 23742–23747.
14. Vallejo, A. N. 1995. Mutagenesis and synthesis of novel recombinant genes using PCR. In *PCR primers*. C. W. Dieffenbach, editor. Cold Springs Harbor Laboratory Press, New York. 603–625.
15. Bligh, E. G. and W. J. Dyer. 1959. A rapid method of total lipid extraction and purification. *Can. J. Biochem. Phys.* **37**: 911–917.
16. Dean, M., Y. Hamon, and G. Chimini. 2001. The human ATP-binding cassette (ABC) transporter superfamily. *J. Lipid Res.* **42**: 1007–1017.
17. Wang, N., D. L. Silver, P. Costet, and A. R. Tall. 2000. Specific binding of ApoA-I, enhanced cholesterol efflux, and altered plasma membrane morphology in cells expressing ABC1. *J. Biol. Chem.* **275**: 33053–33058.
18. Tanaka, A. R., Y. Ikeda, S. Abe-Dohmae, R. Arakawa, K. Sadanami, A. Kidera, S. Nakagawa, T. Nagase, R. Aoki, N. Kioka, T. Amachi, S. Yokoyama, and K. Ueda. 2001. Human ABCA1 contains a large amino-terminal extracellular domain homologous to an epitope of Sjogren's syndrome. *Biochem. Biophys. Res. Commun.* **283**: 1019–1025.
19. Fitzgerald, M. L., A. J. Mendez, K. J. Moore, L. P. Andersson, H. A. Panjton, and M. W. Freeman. 2001. ABCA1 contains an N-terminal signal-anchor sequence that translocates the protein's first hydrophilic domain to the exoplasmic space. *J. Biol. Chem.* **276**: 15137–15145.
20. Clee, S. M., J. J. Kastelein, M. van Dam, M. Marcil, K. Roomp, K. Y. Zwarts, J. A. Collins, R. Roelants, N. Tamasawa, T. Stulc, T. Suda, R. Ceska, B. Boucher, C. Rondeau, C. DeSouich, A. Brooks-Wilson, H. O. Molhuizen, J. Frohlich, J. Genest, Jr., and M. R. Hayden. 2000. Age and residual cholesterol efflux affect HDL cholesterol levels and coronary artery disease in ABCA1 heterozygotes. *J. Clin. Invest.* **106**: 1263–1270.
21. Luciani, M. F., F. Denizot, S. Savary, M. G. Mattei, and G. Chimini. 1994. Cloning of two novel ABC transporters mapping on human chromosome 9. *Genomics.* **21**: 150–159.
22. Fitzgerald, M. L., A. L. Morris, J. S. Rhee, L. P. Andersson, A. J. Mendez, and M. W. Freeman. 2002. Naturally occurring mutations in the largest extracellular loops of ABCA1 can disrupt its direct interaction with apolipoprotein A-I. *J. Biol. Chem.* **277**: 33178–33187.
23. Bungert, S., L. L. Molday, and R. S. Molday. 2001. Membrane topology of the ATP binding cassette transporter ABCR and its relationship to ABC1 and related ABCA transporters. *J. Biol. Chem.* **276**: 23539–23546.
24. Illing, M., L. L. Molday, and R. S. Molday. 1997. The 220-kDa rim protein of retinal rod outer segments is a member of the ABC transporter superfamily. *J. Biol. Chem.* **272**: 10303–10310.
25. Wine, J. J. 1995. Cystic fibrosis: How do CFTR mutations cause cystic fibrosis? *Curr. Biol.* **5**: 1357–1359.
26. Smith, J. D., C. Waelde, A. Horwitz, and P. Zheng. 2002. Evaluation of the role of phosphatidylserine translocase activity in ABCA1 mediated lipid efflux. *J. Biol. Chem.* **277**: 13.
27. Tall, A. R., N. Wang, and P. Mucksavage. 2001. Is it time to modify the reverse cholesterol transport model? *J. Clin. Invest.* **108**: 1273–1275.
28. Haghighpassand, M., P. A. Bourassa, O. L. Francone, and R. J. Aiello. 2001. Monocyte/macrophage expression of ABCA1 has minimal contribution to plasma HDL levels. *J. Clin. Invest.* **108**: 1315–1320.
29. Wellington, C. L., E. K. Walker, A. Suarez, A. Kwok, N. Bissada, R. Singaraja, Y. Z. Yang, L. H. Zhang, E. James, J. E. Wilson, O. Francone, B. M. McManus, and M. R. Hayden. 2002. ABCA1 mRNA and protein distribution patterns predict multiple different roles and levels of regulation. *Lab. Invest.* **82**: 273–283.
30. Luciani, M. F., and G. Chimini. 1996. The ATP binding cassette transporter ABC1, is required for the engulfment of corpses generated by apoptotic cell death. *EMBO J.* **15**: 226–235.
31. Oram, J. F., R. M. Lawn, M. R. Garvin, and D. P. Wade. 2000. ABCA1 is the cAMP-inducible apolipoprotein receptor that mediates cholesterol secretion from macrophages. *J. Biol. Chem.* **275**: 34508–34511.
32. Bertolini, S., L. Pisciotto, M. Seri, R. Cusano, A. Cantafora, L. Calabresi, G. Franceschini, R. Ravazzolo, and S. Calandra. 2001. A point mutation in ABC1 gene in a patient with severe premature coronary heart disease and mild clinical phenotype of Tangier disease. *Atherosclerosis.* **154**: 599–605.
33. Clee, S. M., A. H. Zwinderman, J. C. Engert, K. Y. Zwarts, H. O. F. Molhuizen, K. Roomp, J. W. Jukema, M. van Wijland, M. van Dam, T. J. Hudson, A. Brooks-Wilson, J. Genest, Jr., J. J. P. Kastelein, and M. R. Hayden. 2001. Common genetic variation in ABCA1 is associated with altered lipoprotein levels and a modified risk for coronary artery disease. *Circulation.* **103**: 1198–1205.
34. Wang, J., J. R. Burnett, S. Near, K. Young, B. Zinman, A. J. Hanley, P. W. Connelly, S. B. Harris, and R. A. Hegele. 2000. Common and rare ABCA1 variants affecting plasma HDL cholesterol. *Arterioscler. Thromb. Vasc. Biol.* **20**: 1983–1989.
35. Attie, A. D., J. P. Kastelein, and M. R. Hayden. 2001. Pivotal role of ABCA1 in reverse cholesterol transport influencing HDL levels and susceptibility to atherosclerosis. *J. Lipid Res.* **42**: 1717–1726.
36. van Dam, M. J., E. de Groot, S. M. Clee, G. K. Hovingh, R. Roelants, A. Brooks-Wilson, A. H. Zwinderman, A. J. Smit, A. H. Smelt, A. K. Groen, M. R. Hayden, and J. J. Kastelein. 2002. Association between increased arterial-wall thickness and impairment in ABCA1-driven cholesterol efflux: an observational study. *Lancet.* **359**: 37–42.